
# Cinematographic Analysis of Counter Jet Formation in a Single Cavitation Bubble Collapse Flow


S.-H. Yang, S.-Y. Jaw and K.-C. Yeh



Journal of Mechanics / Volume 27 / Issue 02 / June 2011, pp 253 - 266
DOI: 10.1017/jmech.2011.29, Published online: 16 June 2011

# CINEMATOGRAPHIC ANALYSIS OF COUNTER JET FORMATION IN A SINGLE CAVITATION BUBBLE COLLAPSE FLOW

**S.-H. Yang** [*]

*Department of Civil Engineering*
*National Chiao Tung University*
*Hsinchu, Tainan, Taiwan 30010, R.O.C.*

**S.-Y. Jaw** [**]

*Department of Systems Engineering and Naval Architecture*
*National Taiwan Ocean University*
*Keelung, Taiwan 20224, R.O.C.*

**K.-C. Yeh** [**]

*Department of Civil Engineering*
*National Chiao Tung University*
*Hsinchu, Tainan, Taiwan 30010, R.O.C.*

**ABSTRACT**

This study utilized a U-shape platform device to generate a single cavitation bubble for the detail analysis of the flow field characteristics and the cause of the counter jet during the process of bubble collapse induced by pressure wave. A series of bubble collapse flows induced by pressure waves of different strengths are investigated by positioning the cavitation bubble at different stand-off distances to the solid boundary. It is found that the Kelvin-Helmholtz vortices are formed when the liquid jet induced by the pressure wave penetrates the bubble surface. If the bubble center to the solid boundary is within one to three times the bubble's radius, a stagnation ring will form on the boundary when impacted by the penetrated jet. The liquid inside the stagnation ring is squeezed toward the center of the ring to form a counter jet after the bubble collapses. At the critical position, where the bubble center from the solid boundary is about three times the bubble's radius, the bubble collapse flows will vary. Depending on the strengths of the pressure waves applied, either just the Kelvin-Helmholtz vortices form around the penetrated jet or the penetrated jet impacts the boundary directly to generate the stagnation ring and the counter jet flow. This phenomenon used the particle image velocimetry method can be clearly revealed the flow field variation of the counter jet. If the bubble surface is in contact with the solid boundary, the liquid jet can only splash radially without producing the stagnation ring and the counter jet. The complex phenomenon of cavitation bubble collapse flows are clearly manifested in this study.

**Keywords :** Cavitation bubble, Kelvin-helmholtz vortices, Stagnation ring, Counter jet, Particle image velocimetry.

## 1. INTRODUCTION

It has been known that the collapse of the cavitation bubbles could cause serious destruction of pressure pipes, hydraulic machineries and turbine structures. After the cavitation bubble is generated, the variation of its surrounding velocity and pressure field could result in its collapse. If the process of the collapse of a cavitation bubble appears near the solid boundary, its impact to the boundary could generate an immense water-hammer pressure effect [1]. The shock wave generated in this process of bubble collapse could possibly impact or even destroy the solid boundary of structure.

The possibility of serious structural damage caused by these tiny cavitation bubbles has surely caught the attention and curiosity of researchers. Many of them have plunged into the study of the characteristics of the flow field of bubble collapse and its effect on the deterioration and destruction of its surrounding solid boundary. These studies include the understanding of the shock wave, the characteristics of the resultant luminescence, and the jet related fields. If the cavitation bubble is located near the solid boundary at certain suitable distance, it is more possible for the production of counter-jet in the process of bubble collapse. There has not been a firm conclusion for the exact characteristics which causes the destruction of the interface on the solid boundary.

Rayleigh [2] studied the corrosion of high speed blade subjected to the effect of cavitation bubble. He mentioned that the bubble collapse is able to produce a high speed flow jet which damages the solid surface. During the course of his research, he developed the

[*] Post-Doctoral Research Associate, corresponding author [**] Professor


DOI : 10.1017/jmech.2011.29

pressure dynamic theory for the collapse of spherical bubbles and derived the Rayleigh equation. Many following researchers carried out related researches based on this theory. Among which is Plesset [3] who further considered the influence of the physical characteristics of fluid viscosity and surface tension and derived the Rayleigh-Plesset equation. Gilmore [4] moved forward to consider the influence of the compressibility of fluid on the flow field of the bubble collapse. Plesset and Zwick [5] furthered the research to include the influence of the thermo conductivity of the fluid flow field of the bubble collapse. According to their research results, the time required for the bubble collapse is too short and the influence of the thermo conductivity is kept at minimum. Therefore the bubble collapse can be assumed to be a heat insulated process.

Kornfeld and Suvorov [6] brought up the theory of bubble collapse near a solid boundary. They proposed that the bubble would be deformed to a non-spherical shape with the bubble surface tension penetrated subsequently to generate the phenomenon of flow jet. This phenomenon was proved in the experiment carried out by Naude and Ellis [7]. The numerical model in Plesset and Chapman's research [1] also revealed this phenomenon. If the solid boundary is located on the right side of the bubble, the jet flow would be formed on the left side of the bubble and penetrates it before arriving at the right side interface of the bubble. The damage of the solid boundary might be caused by the impact of this jet flow during the bubble collapse. Benjamin and Ellis [8] and Philipp and Lauterborn [9] also detected the bubble collapse phenomenon and its consequent behavior of damage at the solid boundary. Recent research results reveled that the destructive power of the jet flow was not the main factor for the damage of the solid boundary. However, the jet flow influence which causes the collapse of the bubble is still an important element for the research of the hydrodynamics of the flow field.

Rayleigh [2] first analyzed the theoretical pressure variation of the flow field of the bubble collapse. The bubble collapse results in a very high pressure, forming a shock wave which is sent towards the outside of the bubble. Harrison [10] in his experimental results proved the existence of a noise generated by the collapse of bubble at its surrounding rigid boundary. Vogel and Lauterborn [11] found a close relationship between the strength of the wave pulse and the distance between the position of the bubble and the rigid boundary. This wave pulse could then generate a series of shock waves. This phenomenon was studied and revealed in the experiments carried out by Tomita and Shima; Ward and Emmony; Ohl *et al*.; Shaw *et al*.; Lindau and Lauterborn [12-16].

Light could be emitted in the process of the bubble collapse when the volume of the bubble is compressed to its minimum radius during which the gas inside is heated in a heat-insulated process. For bubbles under low viscosity and high pressure, it is easier for the emission of light. This is because at high viscosity, the time for bubble collapse is increased and the gas inside is not heated to the sufficient temperature to emit light. Ohl *et al*. [17] also found the emission of light near the solid boundary under specific conditions in the process of bubble collapse. This phenomenon is called the "Single Cavitation Bubble Luminescence (SCBL)". Buzukov and Teslenko [18] and Akmanov *et al*. [19] also had similar research reports. The strength of the SCBL is closely related to the distance between the bubble position and its surrounding solid boundary [21]. This relationship might be resulted from the compressibility (under the influence of the distance to the solid boundary) of the bubble. The researches related to the SCBL in recent years included Wolfrum *et al*., Baghdassarian *et al*. [21,22].

Counter jet could be generated when the bubble is located near the solid boundary. The initial formation and increment of the size of the counter jet is very rapid and it could exist for a while. Experiments related to the counter jet is found in Harrison [10] and Kling and Hammitt's [23] researches but it is until Lauterborn [24] who first described the counter jet phenomenon. There has not been a final conclusion for the cause of the generation of the counter jet. Counter jet did not appear in the numerical simulations carried out by Best; Zhang *et al*.; Blake *et al*. [25-27]. However, it appeared in the experiments carried out by Philipp and Lauterborn; Tomita and Shima; Ward and Emmony; Vogel *et al*.; Kodama and Tomita [9,12,13,28,29]. The discrepancy between the numerical simulations and the experimental results leads to the assumption that the counter jet flow field is not part of the bubble collapse process. Its formation might be generated by a complicated mechanism in the fluid during the bubble collapse. For example, if the bubble is in contact with the solid boundary, the counter jet would not be generated. The shock wave generated appears at the final stage of the process of bubble collapse. Since the counter jets also appear at the final stage of the bubble collapse, there are speculations for their possible formation due to the shock wave structure.

In the experiments carried out by Vogel *et al*. [28], the appearance of the counter jet during the bubble collapse is dependent on the distance from the center of the bubble to the solid boundary:

$$\gamma = \frac{d}{R_{\max}} \tag{1}$$

where $R_{\max}$ is the maximum radius and $d$ is the distance between the bubble center and the solid boundary. When $\gamma$ is in the range of $1 < \gamma \approx 3$, counter jet could be observed. However, no counter jet is generated under the condition of $\gamma > 3$. Lindau and Lauterborn [16] discussed on the relationships between the rebound height, the collapse time and their respective $\gamma$ values in the phenomenon of counter jet. These results revealed an increasing $\gamma$ for a smaller rebound height, and a shorter time of collapse.

Best [25] introduced a numerical simulation method for the process of bubble collapse. Tong *et al*. [30] presented the simulation of the flow field of bubble collapse at some different positions. In their analysis,

it appeared that no counter jet was formed when the bubble collapsed in a range of $0.6 < \gamma < 1$. Instead, a splash would be produced after the impinged jet penetrated the bubble surface and subsequently hit the solid boundary. The pressure generated by the splash could have considerable influence on the boundary. The first experimental evidence of such an effect was based on the pressure measurements by Shaw *et al*. [31] Brujan *et al*. [32] used high-speed camera to present a series of images of the toroidal bubble collapse with the splash located in the range between $\gamma$ = 1.1and 0.9. This result was compared to the numerical simulations. Lindau and Lauterborn [16] also presented a series of experimental results regarding the splash in order to obtain an agreement with the numerical simulations. When $\gamma$ was less than 0.6, the fluid layer between the bubble surface and the solid boundary was too thin to form the splash.

According to Rayleigh's equation, when the effect of the surrounding solid boundary is excluded, the relationship between the time of bubble collapse and its radius is:

$$R_{\max} = 1.09\sqrt{\frac{p - p_v}{\rho}}\, t_c \tag{2}$$

where $p$ and $\rho$ are the pressure of the flow field and the fluid density at ambient temperature respectively, $p_v$ is the vapor pressure, $t_c$ is the bubble collapse time. If the solid boundary condition is put into consideration, a greater bubble collapse time is required. Generally the size of the cavitation bubble produced in the laboratory is about 1.5mm in radius. Under ambient temperature, the bubble collapse time ranges from 100μs ~ 200μs. It is not easy to generate cavitation bubbles for their small volumes, short collapse time, and complicated flow fields; all of which contribute to a great difficulty of the measurement. In order to record and analyze the characteristics of the flow field of the bubble collapse, common experimental setup includes a high speed camera with framing rates ranging between several thousand to 100 million frames per second. Some researchers used the method of particle image velocimetry (PIV) to measure the velocity flow field of the process of bubble collapse [28]. However since the volume of the bubble was small and its collapse time was too short, only a rough sketch of the flow field was obtained. Lawson *et al*. [33] applied the PIV method to measure the flow filed of the collapse of a 80mm diameter rubber balloon and compared it with the numerical simulation. Although these results obtained agreement, there is great discrepancy between the flow field features of the collapse of a balloon and a bubble. Jaw *et al*. [34] obtained sound experimental results using soap bubbles filled with smog particle and applied the PIV method to measure flow fields at different phases during the process of bubble collapse.

In laboratory, a single cavitation bubble could be generated in a test tube using a high energy laser beam to focus on a single point [24,35]. In the following years, many related studies utilized this method to generate a single cavitation bubble. Since these bubbles were generated by the high energy laser beam which causes fluid aeration, it was restricted by the strength of the energy provided by the laser. Usually the bubble created using this method has small volume with 1.5mm in radius. In addition, the inside pressure of the bubble was not equivalent to the vapor pressure at ambient temperature. Moreover, since the bubbles were formed by fluid aeration which parted the fluid molecules, there is no re-congealable vapor inside the bubbles to repeat the experiment. Some other researchers used the method of electrolysis to generate a bubble on a platinum electrode at the bottom of a box. However, this method has a defect of disturbing the flow field during the bubble collapse. Another method for forming the bubble is through the use of a needle to inject air into the test tube before using a lithotripter to generate a shock wave up to 94MPa to break the bubble [36]. Sankin *et al*. [37] also used a lithotripter to generate a 39MPa shock wave to break the laser induced bubble in order to measure the flow field of the interaction between the bubble collapse and the shock wave.

From the paper reviews presented above, it is perceived that the cavitation bubble collapse flow is very difficult to measure due to the facts that the bubble size is small, the collapse time is very short, and the flow induced is very complicate. In addition, as mentioned before, the bubble generated by the optical breakdown is different from a true cavitation bubble. A cavitation bubble containing re-condensable vapor, when collapsed, will produce greater energy than the ones without re-condensable vapor [38]. To resolve these problems, a simpler method for the generation of a true cavitation bubble is proposed in this study. By rotating a L tube filled with tap water, a single cavitation bubble is generated and stayed at the center of the rotational axis due to the effect of centrifugal force. The cinematographic analysis of bubble collapse flows induced by pressure waves of different strengths can thus be performed easily. By lowering the strength of the pressure wave, the bubble collapsed in a longer period of time, the characteristics of the true cavitation bubble collapse flow are clearly manifested. Improvement in the further used the PIV method that can be clear revealed velocity flow field feature during the bubble collapse. The present study focuses on the investigation of the formation of the liquid jet and the counter jet, at different stand-off distances to the boundary, and their consequent influences on the bubble collapse flow.

## 2. EXPERIMENT INSTRUMENT AND CAVITATION BUBBLE GENERATOR

The experimental setup for the flow field measurement of cavitation bubble collapse is shown in Fig. 1. This device is consisted of an insulated optical platform, a motor, a rotatable U-shape platform, a transparent cylindrical tube, a set of light sources, a shock wave pressure generator, a high speed camera and a pressure sensor. The LEEDAN DC brushless motor is capable to produce a maximum controlled rotational velocity up to 2,000 RPM, to supply a maximum power up to two

horsepower, and to stop the rotational motion in a relatively short period of time.

The U-shape platform was made up of an acrylic platform of 20mm in thickness. Centered at the rotational axis of the motor, its rotatable arm has a radius of 250mm, which resulted in a total horizontal length of 500mm. Two vertical forearms each of 150mm in height are fixed to the edge of the platform. On the platform of the horizontal rotatable level arm sites the transparent cylindrical tube of 200mm in length, with its internal and external diameter of 5mm and 8mm respectively. A soft PVC tube with an internal diameter of 5mm is fixed to the vertical forearm in order to conveniently exchange the experimental equipment. At one end, this tube is connected to the shock wave pressure generator with a piston while it is extended to connect the transparent cylindrical tube at the other end. At the extremity of the transparent cylindrical tube, a rigid boundary with a 1mm drilled hole is set up to connect the highly sensitive pressure sensor that measures the shock wave pressure at different strengths during the process of the single bubble collapse (shown at the upper part of Fig. 1). On the other hand, the cavitation bubble generation takes place at the site on the platform of the rotational axis where the pressure is at the lowest. Therefore, the transparent cylindrical tube must be located across the center of the rotational axis for easier cavitation bubble generation.

During the experiment of generating a single cavitation bubble, the transparent cylindrical tube on the U-shape platform is filled with tap water shown in Fig. 2. The surface of the fluid at the part of the vertical forearm tube is in touch with air with one atmosphere pressure. Therefore, the center location of the L tube at initial condition has a hydrostatic pressure of $p_0 = p_{\text{atm}} + \rho_g \Delta h$, where $p_{\text{atm}}$ is the atmosphere pressure, g is the acceleration of gravity, and $\Delta h$ is the water depth difference.

When the U-shape platform is rotated by the motor, the fluid is subjected to a centrifugal force resulting in a parabolic fluid pressure distribution shown as the dotted line in Fig. 2 at different radius. At the vertical forearm, although the $\Delta h$ is slightly increased, the hydrostatic water pressure is still kept at one atmospheric pressure because the surface interface is still in touch with the air. Therefore, the pressure difference between the free surface atmospheric pressure and the pressure at the center of rotation is $\rho_g \Delta h - 1/2\rho r^2\omega^2$, where $r$ is the rotational radius and $\omega$ is the rotational velocity. When $\omega$ is gradually increased, the pressure at the center of the rotation in the transparent cylindrical tube is gradually decreased to a saturated vapor pressure at local present water temperature. At this condition, a single cavitation bubble at the rotational center can be generated. The rotational speed needed for generating a cavitation bubble is related to the $\Delta h$. Greater $\Delta h$ means a greater rotational velocity required for the production of cavitation bubble. If $\Delta h$ is kept constant, an increasing rotational velocity would result in a greater size of cavitation bubble. Therefore by controlling the rotational velocity of the U-shape platform, a desirable size of a single cavitaiton bubble could be generated.

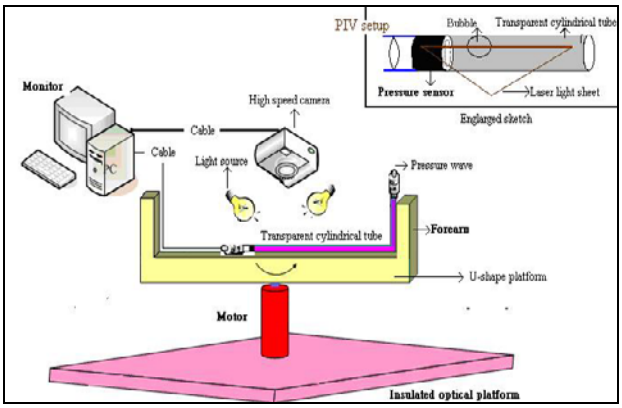


Fig. 1 Schematic diagram of the experiment setup

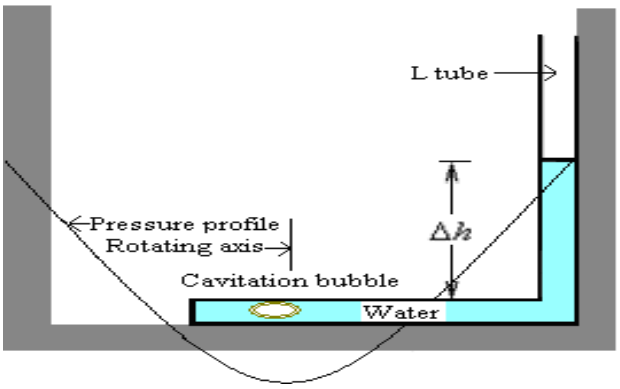


Fig. 2 The pressure distribution for a rotating U-shape platform

After the cavitation bubble is generated, the U-shape platform is stopped to restore the pressure back to the hydrostatic pressure instantly. This pressure difference alone is not enough to break the cavitation bubble. Therefore, in order to observe the flow field of the collapse of the cavitation bubble, this study uses a pulse setup to hit the piston of the PVC soft tube in contact with the free water surface and instantly generates a shock wave pressure sending an impact to cause the collapse of the cavitation bubble. The signal to propel the pulse setup impacting the piston device is triggered while the image data and the pressure profile are recorded and stored by the computer through the high speed camera and the pressure sensor respectively. This experimental setup allows the real-time recording of the time-series relationships between the flow field image data and the pressure change profile with their subsequent analysis.

A Fastec high speed camera is used to extract and record the experimental images. The speed of image extraction is determined by the size of the image. For example, an image extraction speed of 4,000 frame/second is used for an image size of 1280 × 128 pixels. A Kulite XTL-190 pressure sensor incorporating with the NI-6221 Analog I/O device are used for the measurement of the pressure profile. The NI-6221 Analog I/O device can send a 10V signal to drive the pressure sensor and receive a 0 – 0.5V pressure signal to record data which enables itself for the analysis of the pressure change profile in the transparent cylindrical tube.

In addition, the image data is related to the pressure change profile on the basis of the real-time data acquisition. For each image taken by the high speed camera, a 3.2V signal is sent simultaneously from the external output of the camera through a coaxial cable to the NI-6221 device as a receiving end. Through this I/O function a signal is sent to trigger the pressure sensor and finally a pressure signal is sent to the I/O function for recording. When the high speed camera stopped recording the image files, the pressure sensor simultaneously stopped extracting data. Hence every recorded image of the cavitation bubble in its collapse process can be matched with the measured pressure data from the pressure sensor for the recognition of image data with the pressure change profile in the transparent cylindrical tube before taking these data for further related analysis.

On the other hand, PIV method is used Argun laser pass a transparent cylindrical glass to form a light sheet and in the liquid arranged TSI glass bead-hollow particle (8 ~ 12μm) to assist the camera catch the particle image during the cavitation bubble collapse process, as shown in upper right schematic diagram in Fig. 1. The light sheet thickness is 1.5mm pass the bubble location and the camera catch the bubble collapse image process then record a cinematograph file. After this file is transfer to several sequence particle image data. Using the particle images and the PIV analysis method can obtain the velocity flow field feature during the bubble collapse process. Therefore, a single cavitation bubble and the subsequent bubble collapse flows induced by pressure waves are easily generated by the experimental setup proposed in this study. Cinematographic analysis of the cavitation bubble collapse flows at different stand-off distances are performed and discussed in the following.

## 3. FLOW FIELD MEASUREMENT OF THE COLLAPSE OF CAVITATION BUBBLES

It is found that the presence of the solid boundary has distinct influence on the flow field of a pressurized cavitation bubble and its final collapse. A distance parameter $\gamma$ is assigned to represent the distance from the center of the bubble to the solid boundary. Pressure wave at different strengths are applied to break the bubble. The results are described below:

### 3.1 Flow Field Measurement of Bubble Collapse at $\gamma \approx 7$

Under this condition, the distance between the center of the cavitation bubble and the solid boundary is nearly seven time of its radius. The flow field of the process of cavitation bubble collapse is not affected by the solid boundary. Therefore the solid boundary is assumed to be insignificant to the process of bubble collapse. This process of the cavitation bubble being pressurized followed by its final collapse is shown in Fig. 3. The pressure wave is sent from the left side of the bubble surface, impacting the bubble with peak strength up to 160kPa. The pressure wave caused a concaved deformation of the bubble shown in the first row of Fig. 3.

As shown in Fig. 4, when the bubble is concaved by the pressure wave, a liquid jet is formed at the central axis of the bubble. Initially the liquid jet is converged as the bubble surface concaved toward the center of the bubble. The left hand side bubble surface progressively moves toward the right hand side surface of the bubble. The counter force opposing the liquid jet is then gradually increased as the two bubble surfaces approach each other. At the same time, the liquid jet is accumulating energy and forming a structure that has a larger front and a smaller rear, as shown in second row of Fig. 4.

When sufficient energy is accumulated by the liquid jet during its continuous motion to the right side of the bubble, the overlaid surface is squeezed and subsequently spouted into a jet flow. When the jet flow extended to the static fluid at the right side of the bubble, rapid variation in the flow velocity is created which leaded to a Kelvin-Helmholtz vortex shown in images listed in the second and the third row of Fig. 3. Jaw *et al*. [34] clearly described the Kelvin-Helmholtz vortex, indicating that the interaction between the pressure and the velocity variation is the main cause of this phenomenon.

The bubble collapse process is a complicated and three dimension flow structures. Using the 2D PIV analysis method was lacked a vertical direction motion measurement. In other word, during the bubble surface was pressured to touch the solid boundary, the pressure is uniformly distributed across the tube area, the bubble deformation was approximate a symmetrical development condition. Under this condition, using a high speed camera and 2D PIV method could be obtained flow field. Figure 5 show the velocity flow field of the Kelvin-Helmholtz vortex formation process that used the PIV method to obtain flow field variation during the liquid jet to form vortex formation. The jet flow instantaneously spouted into the static fluid that cause between the jet flow and static fluid shear force difference increased, then the Kelvin-Helmholtz vortex formation is generated, as shown in Fig. 5. From these series of images, the features of the cavitation bubble collapse without solid boundary effect are clearly manifested.

### 3.2 Flow Field Measurement of Bubble Collapse at $\gamma \approx 2$

As described in the introduction, the counter jet would be generated when the distance between the center of the bubble and the solid boundary is within one to three times the bubble's radius ($1 < \gamma \approx 3$). The experiments conducted with $\gamma \approx 2$ falls within this range.

The distance from the right side of the bubble surface to the solid boundary is only one radius long. The Kelvin-Helmholtz vortex was generated after the bubble surface is broken and the jet flow is formed.

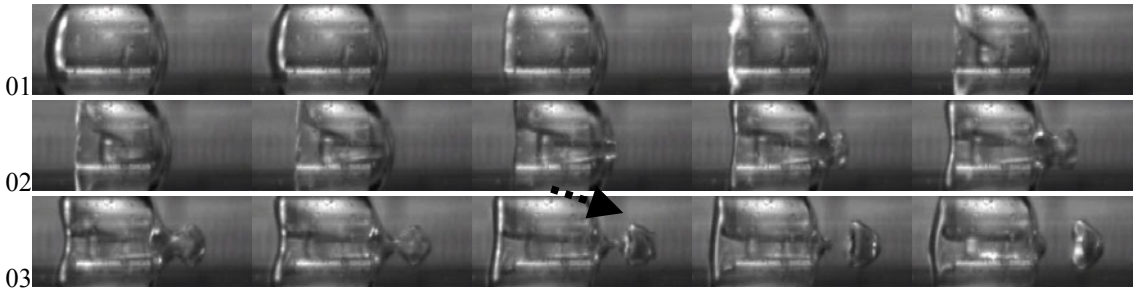


Fig. 3 Top view of images of the process of bubble collapse at $\gamma \approx 7$. 1st row: Image of the inward dent process; 2nd and 3rd rows: Images of the Kelvin-Helmholtz vortex process (the Kelvin-Helmholtz vortex is indicated by a dotted line with an arrow). The peak strength of the pressure wave is 115kPa. Image interval time is 1/2000 second. The size of each individual frame is 10.8mm × 3.1mm. The bubble $R_{max}$ is 2.5mm. ($\Delta h$: 55mm, $\omega$: 200RPM)

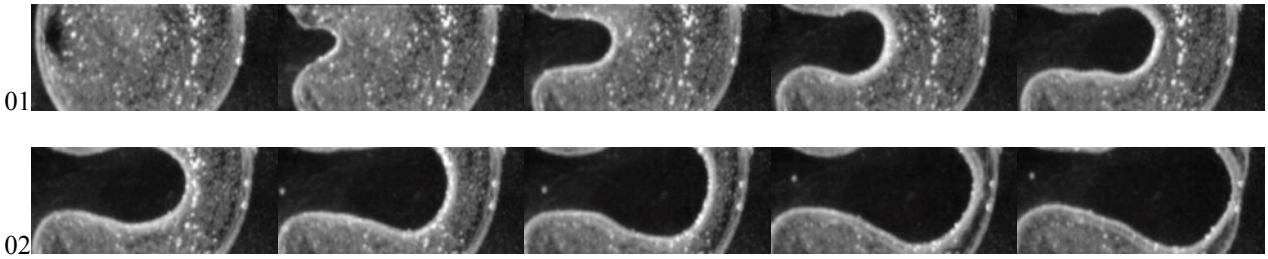


Fig. 4 Liquid jet accumulating energy in the inward dent formed a larger front and a smaller rear shape. The peak strength of the pressure wave is 60kPa. Image interval time is 1/100 second. The size of each individual frame is 8.0mm × 3.0mm. The bubble $R_{max}$ is 3.5mm

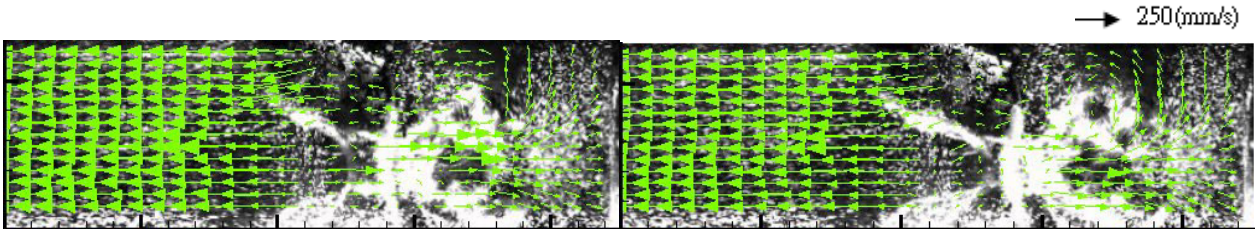


Fig. 5 Exhibit the PIV measurement results at $\gamma \approx 7$. (The velocity flow field of the Kelvin-Helmholtz vortex formation process) The peak strength of the pressure wave is 155kPa. Image interval time is 1/4000 second. The size of each individual frame is 11.0mm × 3.1mm. The bubble $R_{max}$ is 2. 3mm. ($\Delta h$: 53mm, $\omega$: 190RPM)

This vortex would touch the solid boundary and subsequently form the stagnation ring on the solid boundary shown in the left front view diagram in Fig. 6. After the stagnation ring touched the solid boundary, it was divided into two fluid flows. One of them was outside the stagnation ring splashing outwardly along the radial direction. The other fluid flow inside the stagnation ring was squeezed inwardly along the central direction to form a counter jet shown in the lower right side of the diagram in Fig. 6. The preexistence of fluid between the bubble surface and the solid boundary allowed the fluid inside the stagnation ring to be squeezed towards the center resulting in a counter jet. Therefore in order to generate a counter jet, the bubble should be located at $\gamma > 1$ so that there would be enough space between the bubble surface and the solid boundary.

On the other hand, after the bubble surface was penetrated to form the Kelvin-Helmholtz vortex, a zone with high velocity and low pressure was formed at the root of the central axis of the vortex where the bubble was stretched and deformed towards its right side shown in the images at the second row of Fig. 6. In the first image at the third row of Fig. 6, a counter jet located at the central axis of the bubble could be clearly seen.

Many researchers who studied the counter jet have mentioned the existence of the stagnation ring. However, in these studies, the time for the collapse of the bubble was too short for the appearance of the Kelvin-Helmholtz vortex. The relationship between the stagnation ring and the Kelvin-Helmholtz vortex was still not clear. In this study, the process for the formation of the Kelvin-Helmholtz vortex and the counter jet was clearly revealed for a shock wave of lower pressure was utilized to impact the cavitaiton bubble. If the strength of the pressure wave is increased, the resultant counter jet could penetrate the cavitation bubble and subsequently separated the bubble into a number of small bubbles as shown in Fig. 7. In the first image at the second row of Fig. 7, a counter jet located at the central axis of the bubble could be clearly seen.

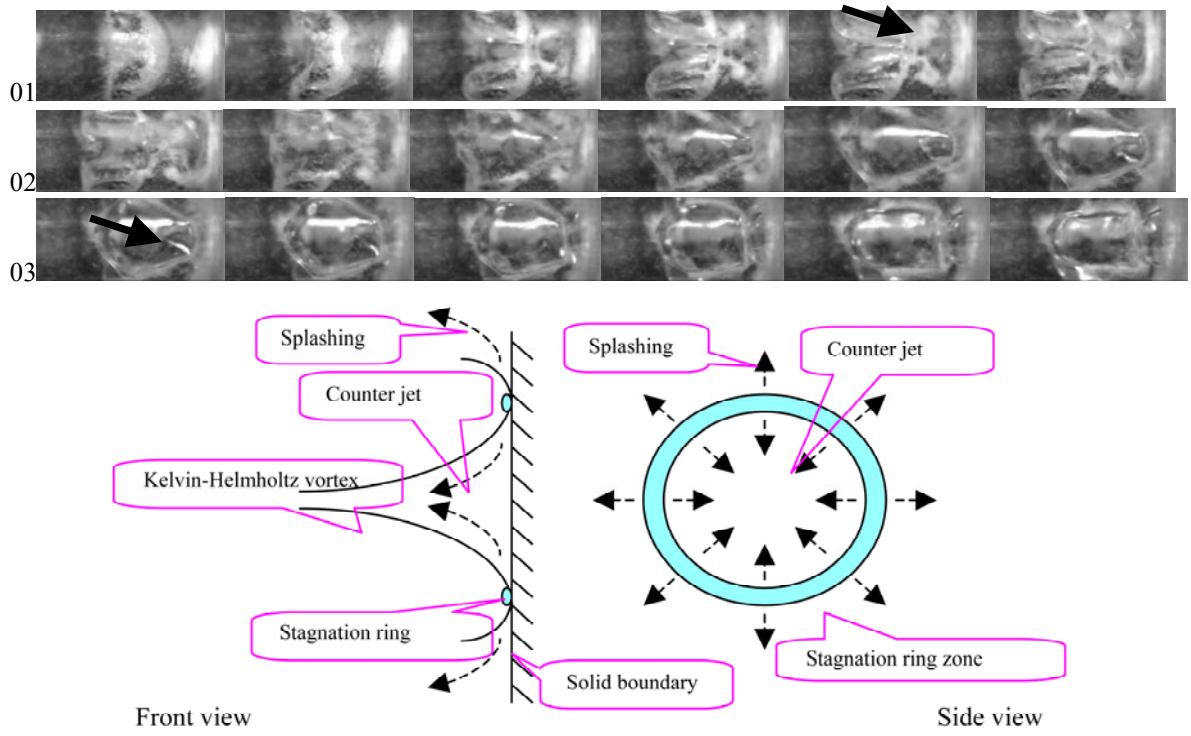


Fig. 6 Upper Part: The process of bubble collapse at $\gamma \approx 2$ (the Kelvin-Helmholtz vortex is indicated by a dotted line with an arrow, the counter jet indicated by a solid line with an arrow). The peak strength of the pressure wave is 250kPa. The image time interval is 1/2000 second. The size of each individual frame is 6.7mm × 3.1mm. $R_{max}$ is 2.0mm. ($\Delta h$: 50mm, ω: 170RPM) Lower Part: Sketch of Kelvin-Helmholtz vortex forming the counter jet

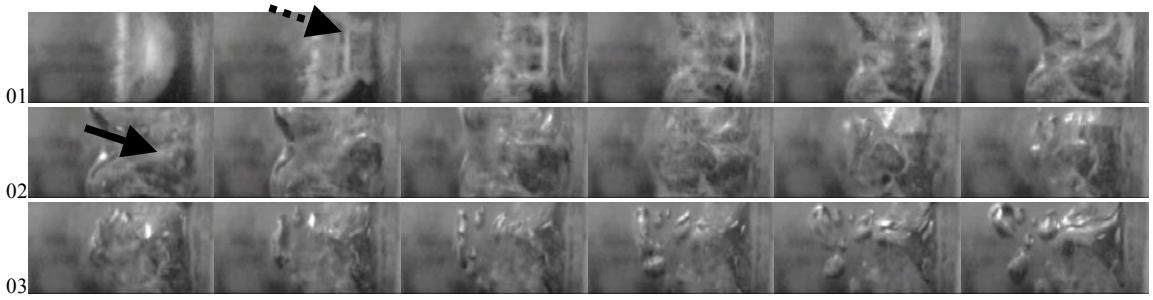


Fig. 7 Images of the process of bubble collapse at $\gamma \approx 2$ with image time interval of 1/2000 second. The peak strength of the pressure wave is 475kPa. The size of each individual frame is 9.0mm × 3.1mm (the Kelvin-Helmholtz vortex is indicated by a dotted line with an arrow; the counter jet indicated by a solid line with an arrow). $R_{max}$ is 2.5mm. ($\Delta h$: 60mm, ω: 225RPM)

Figure 8 show image and the velocity flow field from the Kelvin-Helmholtz vortex touch to the solid boundary and transfer to form the counter jet formation which used the PIV method to obtain velocity flow field variation. After the Kelvin-Helmholtz vortex touch solid boundary, the vortex is formed a planiform shape bubble along the solid boundary, and meantime the vortex formed a radial direction outward splashed out motion, as shown in upper left image and calculation result of Fig. 8. Following by the bubble on the forward stretched effect and between the bubble and solid boundary space restriction conditions, the Kelvin-Helmholtz vortex at center part splash out are restricted and caused the velocity gradually decreased to stagnation at near the solid boundary center, as shown in upper right image and calculation result of Fig. 8. Finally, the stagnation ring and counter jet are formed as shown in lower image and calculation results of Fig. 8. They can be clear revealed that the stagnation ring location and counter jet motion that shown in Fig. 9. The stagnation ring formation is located at a turning point of the velocity vectors near the solid boundary. The counter jet formation is located at between two stagnation rings. The above-mentioned of the PIV calculation results reveal that the stagnation ring and the counter jet formation identically with Fig. 6 lower part schematic diagram.

### 3.3 Flow Field Measurement of Bubble Collapse at $\gamma \approx 3$

The generation of the counter jet needs to satisfy the condition of $1 < \gamma \approx 3$. A critical value of $\gamma \approx 3$ is found to be a decisive value for the generation of a

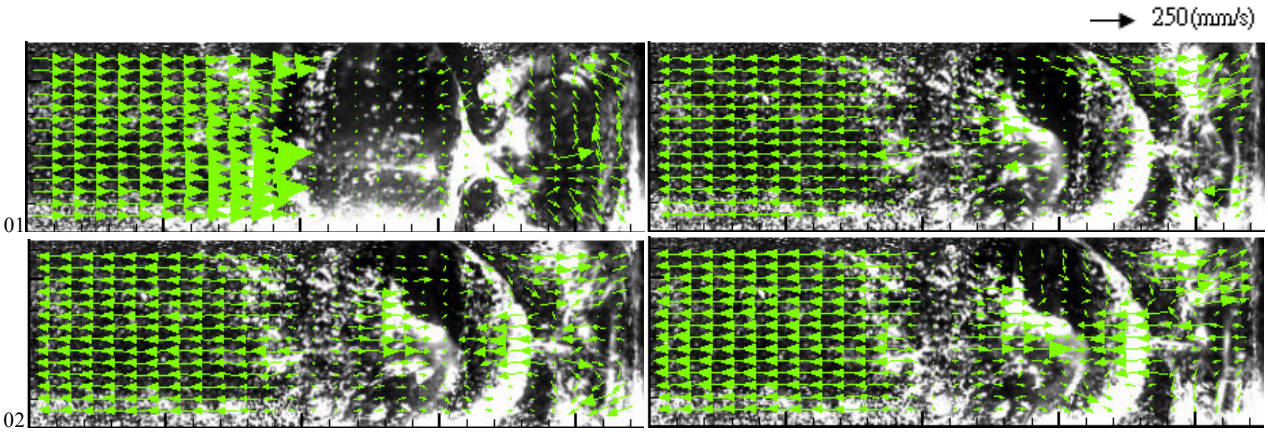


Fig. 8 Exhibit the PIV measurement results at $\gamma \approx 2$. (The velocity flow field of the Kelvin-Helmholtz vortex formation process) The peak strength of the pressure wave is 260kPa. Image interval time is 1/4000 second. The size of each individual frame is 11.0mm × 3.1mm. The bubble $R_{max}$ is 2.3mm. ($\Delta h$: 53 mm, ω: 190 RPM)

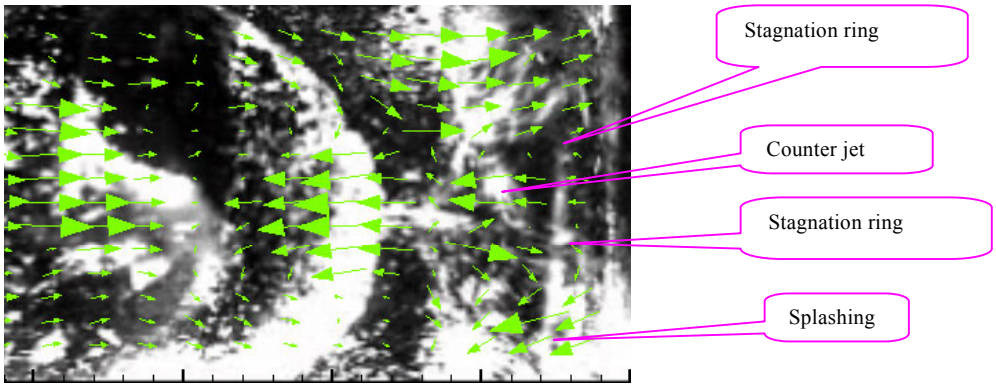


Fig. 9 The velocity flow field is the Fig. 8 lower left diagram near solid boundary enlarged result that can reveal the stagnation ring location, splashing and the counter jet formation.

counter jet. In this study, three different strengths of pressure waves were used to trigger the breakdown the cavitation bubble. Flow field observation for this process of the collapse of cavitation bubble is carried out under this critical condition.

The images located at the first and second row of Fig. 10 revealed the flow field of bubble collapse under a pressure wave of 195kPa in strength. A liquid jet was formed followed by penetrating the bubble surface to produce the jet flow and the Kelvin-Helmholtz vortex. The bubble was divided into two small bubbles because the Kelvin-Helmholtz vortex did not touch the solid boundary. This process of collapse was similar to the case at $\gamma \approx 7$ where the counter jet was not generated.

The process of the collapse of the bubble, with the strength of pressure wave increased to 265kPa, is shown from the third to the sixth rows in Fig. 10. Unlike the semi-hemispheric form of the Kelvin-Helmoholtz vortex shown in the first and second rows of Fig. 10, the vortex shown here was clearly influenced by the solid boundary when the liquid jet penetrated the bubble surface. The right side of the head of the vortex touched the solid boundary and turned into a planiform shape before splashing and spreading outwardly along its surrounding interface. On the other hand, before the head of the vortex touched the solid boundary, the outer ring of the vortex had already touched the tube wall and started spreading outwardly shown in the images at the third row in Fig. 10. This spreading vortex kept moving towards the right side until it touched the solid boundary and generated a subsequent shock wave which rebounded to produce the phenomenon of Richtmyer- Meshkov instability shown near the solid boundary in every image at the fourth row of Fig. 10. Although the Kelvin-Helmholtz vortex could be generated under this strength of pressure wave, the vortex had already splashed and touched the surrounding solid boundary, disabling the vortex from forming the stagnation ring and the counter jet. At the end of this process, the bubble was divided by the liquid jet and the root of the vortex into two smaller bubbles shown in the images at the fifth and sixth rows in Fig. 10.

If the strength of the pressure wave is increased to a peak value of 550kPa, the Kelvin-Helmholtz vortex would touch the solid boundary before the formation of the stagnation ring and the counter jet. This process is shown in the image listed at the seventh and eighth rows of Fig. 10.

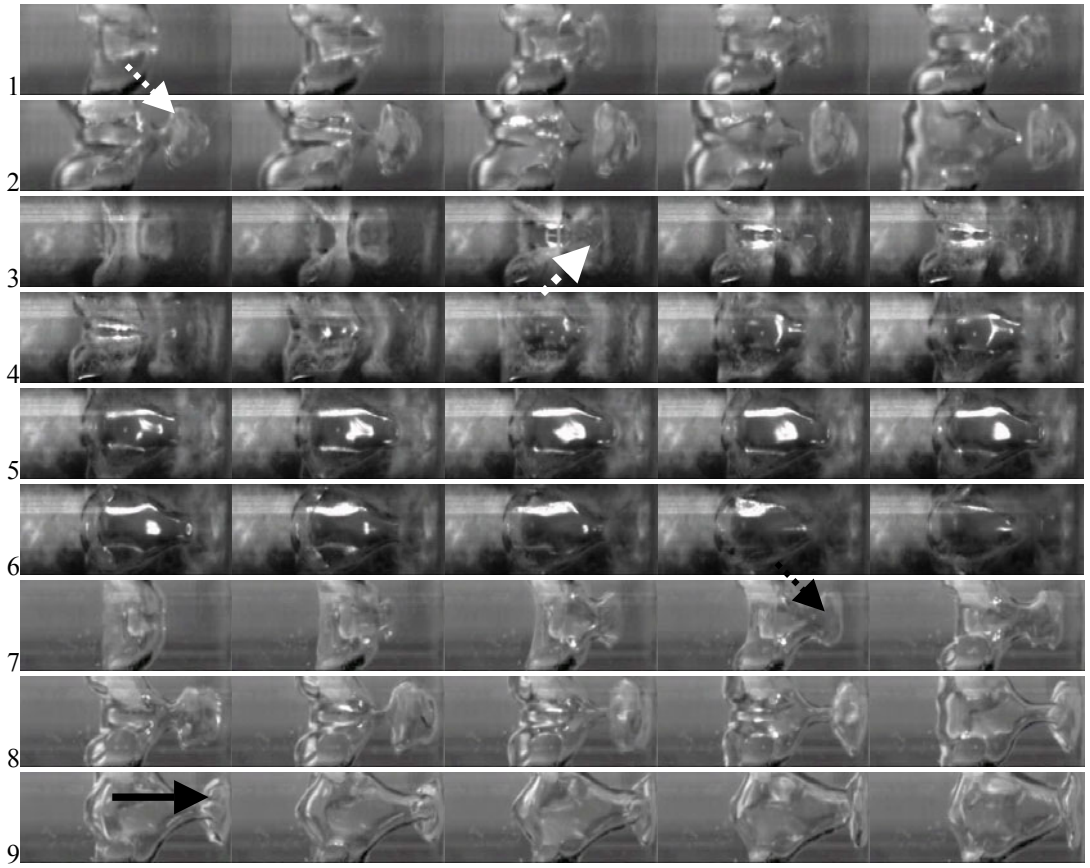


Fig. 10 Images of the process of bubble collapse at $\gamma \approx 3$. The peak strength of the pressure wave for A: 195kPa, B: 265kPa, C: 360kPa. The size of each individual frame for A: 10.5mm × 3.1mm; B: 10.3mm × 3.1mm; C: 9.6mm × 3.1mm. $R_{max}$ for A: 2.45mm; B: 2.35mm; C: 2.25mm. $\Delta h$ for A: 60mm; B: 55mm; C: 50mm. $\omega$ for A: 225RPM; B: 195RPM; C: 175RPM. The image time interval is 1/2000 second. (The Kelvin-Helmholtz vortex is indicated by a dotted line with an arrow; the counter jet is indicated by a solid line with an arrow)

### 3.4 Flow Field Measurement of Bubble Collapse at $\gamma \approx 1$ and $\gamma = 1$

The other critical value for the formation of the counter jet occurs at $\gamma \approx 1$ where the bubble is tightly close to the solid boundary. In this study, in order to understand the characteristics of the flow fields under this critical condition, measurements of flow fields at both locations where $\gamma$ is slightly greater than and equal to one were carried out.

1. When the bubble is located at $\gamma$ slightly greater than 1, there would be a small distance between the bubble surface and the rigid boundary. When the bubble was pressurized and concaved inward, the bubble become more planiform in shape for this deformation was caused by the solid boundary. The area of inward concaved bubble is larger than the three cases mentioned before. After the liquid jet penetrated the bubble surface, there is not enough space to form a complete Kelvin-Helmholtz vortex. However, the space between the bubble surface and the solid boundary would still exist a gap allow the formation of stagnation ring after the liquid jet touches the solid boundary. This is followed by an outward splash along the radial direction while the inward stagnation ring was squeezed along the central direction to form the counter jet. Finally the bubble was divided into two smaller bubbles by the counter jet shown in the image and diagram in Fig. 11. In the further, using PIV calculation results shown in Fig. 12. This result are clear revealed that the liquid jet direct touch the solid boundary and then form the stagnation ring and the counter jet formation.
2. Under the condition of $\gamma = 1$, the bubble interface was pressurized to form an inward concaved bubble. It was followed by the overlaying of the bubble interfaces on the solid boundary without any spaces left for the fluid. After the liquid jet impacted the solid boundary, it just moved outwardly as a splash along the radial direction. The bubble collapses subsequently on the radial trajectory without forming of the stagnation ring and the inwardly squeezed counter jet. This process of bubble collapse is shown in the images and diagrams in Fig. 13

## 4. CONCLUSIONS

In this study, a single cavitation bubble is generated by rotating a L-tube filled with water; the pressure at the rotating axis of the L-tube is lowered to the water vapor pressure due to the centrifugal acceleration, and

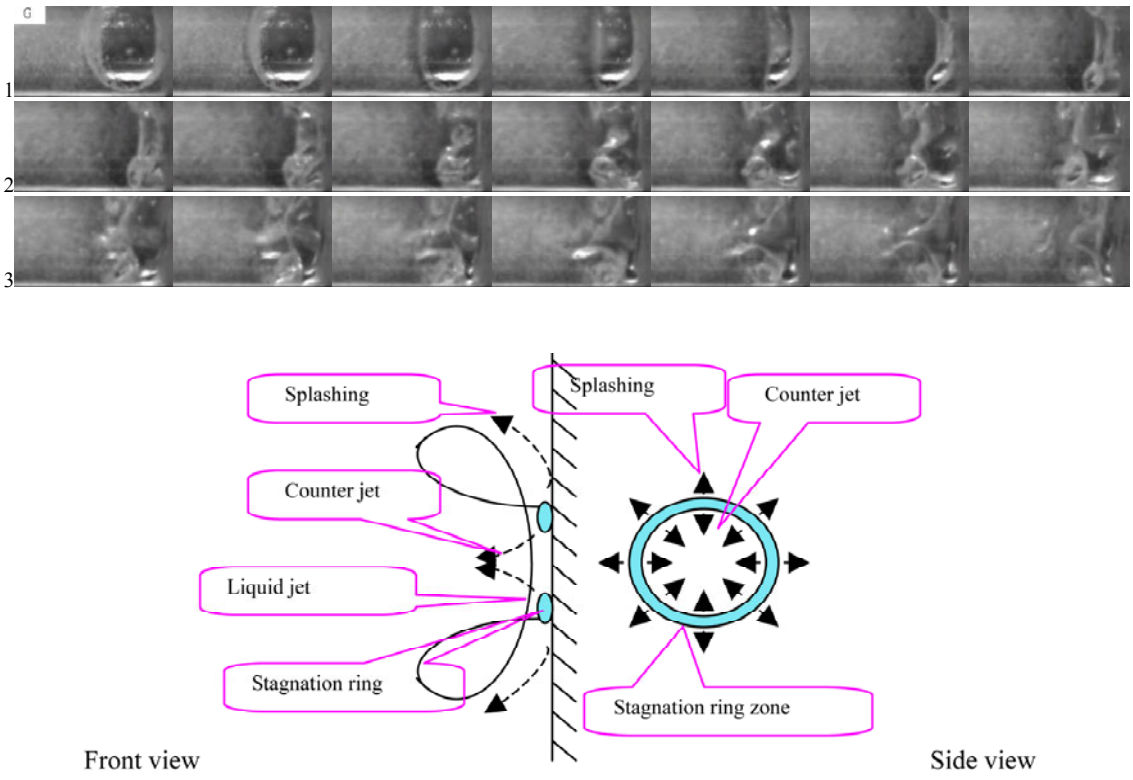


Fig. 11 Upper Part: Images of the process of bubble collapse at $\gamma = 1$; the peak strength of the pressure wave is 320kPa; the image time interval is 1/2000 second. The size of each individual frame is 7.6mm × 3.1mm. $R_{max}$ is 2.0mm. ($\Delta h$: 53mm, ω: 180RPM) Lower Part: Sketch of the liquid jet position. (Note: Left diagram of lower part: The solid line is the bubble surface and the dotted line with an arrow is the splashing)

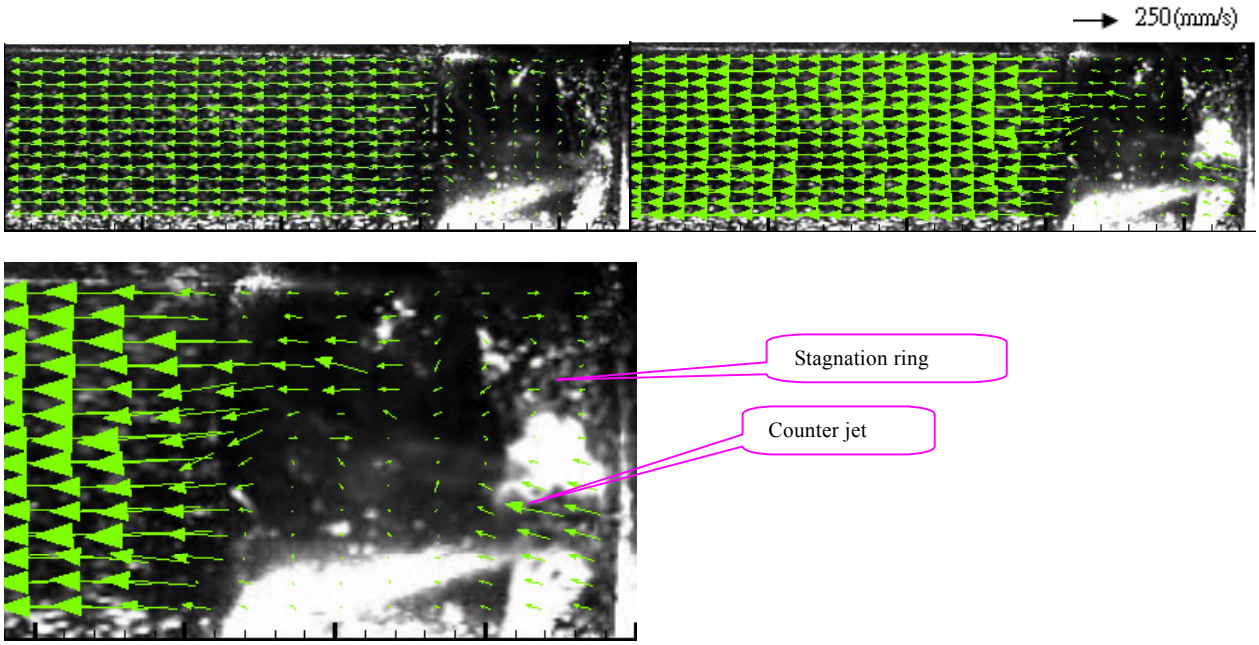


Fig. 12 Upper Part: Exhibit the PIV measurement results at $\gamma \approx 1$. The peak strength of the pressure wave is 230kPa. Image interval time is 1/4000 second. The size of each individual frame is 11.0mm × 3.1mm. The bubble $R_{max}$ is 2.35mm. ($\Delta h$: 55mm, ω: 195RPM) Lower part: Exhibit the upper right diagram near solid boundary enlarged the result that can reveal the stagnation ring location and the counter jet formation. (Note: The velocity vectors near the solid boundary are the particle motion results, not from the solid boundary extra velocity boundary condition)

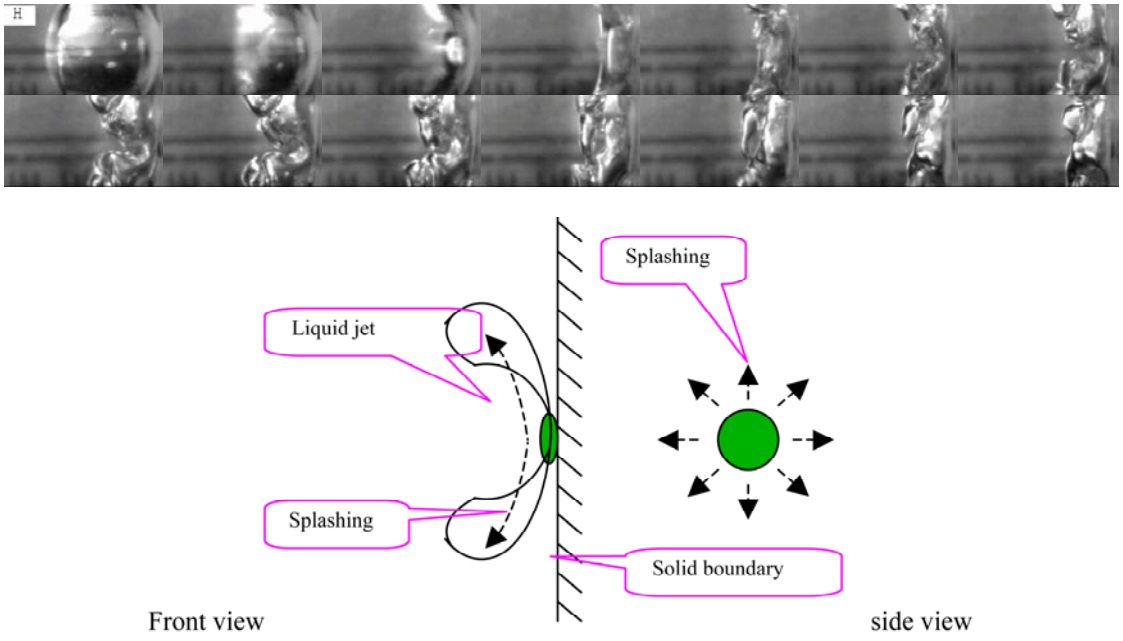


Fig. 13 Upper Part: Images of the process of bubble collapse at $\gamma = 1$; the peak strength of the pressure wave is 520kPa; the image time interval is 1/2000 second. The size of each individual frame is 6.2mm × 3.1mm. $R_{max}$ is 2.25mm. ($\Delta h$: 50mm, $\omega$: 175RPM) Lower Part: Sketch of the liquid jet position

the cavitation bubble is generated right at the rotating axis. The bubble collapse flows are induced by the pressure waves of different strengths. Sequential images of the bubble collapse flow are recorded by a high speed camera. The characteristics of the cavitation bubble collapse flow are clearly manifested by the cinematographic analyses.

For a large stand-off distance, $\gamma \approx 7$, the bubble collapsed without solid boundary influence, a liquid jet is formed due to the bubble deformation. The liquid jet then penetrates the bubble surface. The Kelvin-Helmholtz instability occurs around the penetrated jet surface and vortices are formed due to the presence of sufficient velocity shear between the jet flow and the surrounding static fluid. Counter jet is not formed for such a stand-off distance.

For the stand-off distance, $\gamma \approx 2$, which falls within the range $1 < \gamma \leq 3$, the penetrated jet is capable to impact the solid boundary. A stagnation ring is formed on the solid boundary which separates the jet into an outwards and inwards radial flow. The liquid between the bubble surface and the solid boundary is squeezed by the inwards radial flow to form the counter jet.

At the critical stand-off distance, $\gamma \approx 3$, whether the counter jet occurs depends on the strength of the pressure wave used to induce the bubble collapse. For a lower strength pressure wave, the liquid jet penetrates the bubble but is not able to impact the solid boundary. Neither stagnation nor counter jet can be generated. For an intermediate strength pressure wave, the penetrated jet spread radially so that the circumference of the jet touch the tube wall before the jet front impacts the solid boundary. Neither stagnation ring nor counter jet can be generated. If the strength of the pressure wave is further increased, the penetrated jet is able to impact the solid boundary directly to form the stagnation ring and the counter jet.

For the stand-off distance $\gamma$ slightly greater than 1, a thin liquid layer exists in the small gap between the bubble surface and the solid boundary. The penetrated jet impacts the boundary directly. The stagnation ring is formed on the solid boundary. The thin liquid layer inside the stagnation ring is squeezed by the inwards radial flow to form the counter jet. If $\gamma$ is equal to 1, the bubble surface is in contact with the solid boundary, the liquid jet can not penetrate the bubble but splashes along the radial direction without forming the stagnation ring and the counter jet.

For all the experiments performed in this study, the strength of the pressure wave adopted to induce the bubble collapse flow was kept as low as possible so that the bubble collapsed in a longer period of time. The characteristics of the bubble collapse flows at different stand-off distances can thus be clearly manifested. However, different strengths of the pressure waves are needed to induce the bubble collapse flow at different $\gamma$ locations. A lower strength of the pressure wave is needed for an increasing $\gamma$ value and vice versa.

## REFERENCES

1. Plesset, M. S. and Chapman, R. B., "Collapse of an Initially Spherical Vapour Cavity in the Neighbourhood of a Solid Boundary," *Journal of Fluid Mechanics,* **47**, pp. 283–290 (1971).
2. Raleigh, L., "On the Pressure Developed in a Liquid During the Collapse of a Spherical Cavity," *Philosophical Magazine*, **34**, pp.94–98 (1917).
3. Plesset, M. S., "The Dynamics of Cavitation Bubbles," *Transactions, ASME: Journal of Applied Mechanics*, **16**, pp. 277–282 (1949).

*chanics*, **16**, pp. 277–282 (1949).
4. Gilmore, F. R., "The Growth and Collapse of a Spherical Bubble in a Viscous Compressible Liquid," Technical Report California Institute of Technology, Pasadena, CA (1952).
5. Plesset, M. S. and Zwick, S. A., "A Nonsteady Heat Diffusion Problem with Spherical Symmetry," *Journal of Applied Physics*, **23**, pp. 95–98 (1952).
6. Kornfeld, M. and Suvorov, L., "On the Destructive Action of Cavitation," *Journal of Applied Physics*, **15**, pp. 495–506. (1944).
7. Naude, C. F. and Elli, A. T., "On the Mechanism of Cavitation Damage by Nonhemispherical Cavities Collapse in Contact with a Solid Boundary," *Transactions, ASME D, Journal of Basic Engineering*, **83**, pp. 648–656 (1961).
8. Benjamin, T. B. and Ellis, A. T., "The Collapse of Cavitation Bubbles and the Pressures Thereby Produced Against Solid Boundaries," *Philosophical Transactions of the Royal Society of London Series A, Mathematical and Physical Sciences*, **260**, pp. 221–240 (1966).
9. Philipp, A. and Lauterborn, W., "Cavitation Erosion by Single Laser-Produced Bubbles," *Journal of Fluid Mechanics*, **361**, pp. 75–116 (1998).
10. Harrison, M., "An Experimental Study of Single Bubble Cavitation Noise," *Journal of the Acoustical Society of America*, **24**, pp. 776–782 (1952).
11. Vogel, A. and Lauterborn, W., "Time-Resolved Particle Image Velocimetry Used in the Investigation of Cavitation Bubble Dynamics," *Applied Optics*, **29**, pp. 1869–1876 (1988).
12. Tomita, Y. and Shima, A., "Mechanisms of Impulsive Pressure Generation and Damage Pit Formation by Bubble Collapse," *Journal of Fluid Mechanics*, **169**, pp. 535–564 (1986).
13. Ward, B. and Emmony, D. C., "Direct Observation of the Pressure Developed in a Liquid During Cavitation-Bubble Collapse," *Applied Physics Letters*, **59**, pp. 2228–2231 (1991).
14. Ohl, C. D., Philipp, A. and Lauterborn, W., "Cavitation Bubble Collapse Studied at 20 Million Frames Per Second," *Annalen Der Physik*, **4**, pp. 26–34 (1995).
15. Shaw, S. J., Jin, Y. H., Schiffers, W. P. and Emmony, D. C., "The Interaction of a Single Laser-Generated Cavity in Water with a Solid Surface," *The Journal of the Acoustical Society of America*, **99,** pp. 2811–2824 (1996).
16. Lindau, O. and Lauterborn, W., "Cinematographic Observation of the Collapse and Rebound of a Laser-Produced Cavitation Bubble Near a Wall," *Journal of Fluid Mechanics*, **479**, pp. 327–348 (2003).
17. Ohl, C. D., Lindau, O. and Lauterborn, W., "Luminescence from Spherically and Aspherically Collapsing Laser Induced Bubbles," *Physical Review Letters*, **80**, pp. 393–397 (1998).
18. Buzukov, A. A. and Teslenko, V. S., "Sonoluminescence Following Focusing of Laser Radiation Into Liquid," *Journal of Experimental and Theoretical Physics Letters*, **14**, pp. 189–191 (1971).
19. Akmanov, A. G., Ben'kovskii, V. G., Golubnichii, P. I., Maslennikov, S. I. and Shemanin, V. G., "Laser Sonoluminescence in a Liquid," *Soviet Physics Acoustics*, **19**, pp. 417–418 (1974).
20. Ohl, C. D., Kurz, T., Geisler, R., Lindau, O. and Lauterborn, W., "Bubble Dynamics, Shock Waves and Sonoluminescence," *Philosophical Transactions: Mathematical, Physical and Engineering Sciences*, **357,** pp. 269–294 (1999).
21. Wolfrum, B., Kurz, T., Lindau, O. and Lauterborn, W., "Luminescence of Transient Bubbles at Elevated Ambient Pressure," *Physical Review E*, **64**, pp. 046306 (2001).
22. Baghdassarian, O., Chu, H. C., Tabbert, B. and Williams G. A., "Spectrum of Luminescence from Laser-Created Bubbles in Water," *Physical Review Letters*, **86**, pp. 4934–4937 (2001).
23. Kling, C. L. and Hammitt, F. G., "A Photographic Study of Spark-Induced Cavitation Bubble Collapse," *Transactions of the ASME D: Journal of Basic Engineering*, **94**, pp. 825–833(1972).
24. Lauterborn, W., "Kavitation Durch Laserlicht," *Acustica,* **31**, pp. 52–78 (1974).
25. Best, J. P., "The Formation of Toroidal Bubbles Upon the Collapse of Transient Cavities," *Journal of Fluid Mechanics*, **251**, pp. 79–107 (1993).
26. Zhang, S., Duncan, J. H. and Chahine, G. L., "The Final Stage of the Collapse of a Cavitation Bubble Near a Rigid Wall," *Journal of Fluid Mechanics*, **257**, pp. 147–181 (1993).
27. Blake, J. R., Hooton, M. C., Robinson, P. B. and Tong, R. P., "Collapsing Cavities, Toroidal Bubbles and Jet Impact," *Philosophical Transactions Mathematical, Physical and Engineering Sciences*, **355**, pp. 537–550 (1997).
28. Vogel, A., Lauterborn, W. and Timm, R., "Optical and Acoustic Investigations of the Dynamics of Laser-Produced Cavitation Bubbles Near a Solid Boundary," *Journal of Fluid Mechanics*, **206**, pp. 299–338 (1989).
29. Kodama, T. and Tomita, Y., "Cavitation Bubble Behavior and Bubble-Shock Wave Interaction Near a Gelatin Surface as a Study of in Vivo Bubble Dynamics," *Applied Physical B*, **70**, pp. 139–149 (2000).
30. Tong, R. P., Schiffers, W. P. and Blake, S. J., "Splashing in the Collapse of a Laser-Generated Cavity Near a Rigid Boundary," *Journal of Fluid Mechanics*, **380,** pp. 339–361 (1999).
31. Shaw, S. J., Schiffers, W. P. and Emmony, D. C., "Experimental Observations of the Stress Experienced by a Solid Surface When a Laser-Created Bubble Oscillates in its Vicinity," *Journal of the Acoustical Society of America*, **110**, pp. 1822–1827 (2001).
32. Brujan, E. A., Keen, G. S., Vogel, A. and Blake, J. R., "The Final Stage of the Collapse of a Cavitation Bubble Close to a Rigid Boundary," *Physics of Flu-*

*ids*, **14**, pp. 85–92 (2002).
33. Lawson, N. J., Rudman, A., Guerra, J. and Liow, J. L., "Experimental and Numerical Comparisons of the Break-Up of a Large Bubble," *Experiments in Fluids*, **26**, pp. 524–534 (1999).
34. Jaw, S. Y., Chen, C. J. and Hwang, R. R., "Flow Visualization of Bubble Collapse Flow," *Journal of Visualization*, **10**, pp. 21–24 (2007).
35. Lauterborn, W., "High-Speed Photography of Laser-Induced Breakdown in Lquids," *Applied Physical Letters*, **21**, pp. 27–29 (1972).
36. Philipp, A., Delius, M., Scheffczyk, C., Vogel, A. and Lauterborn, W., "Interaction of Lithotripter-Generated Shock Waves with Air Bubbles," *Journal of the Acoustical Society of America,* **93**, pp. 2496–2509 (1993).
37. Sankin, G. N., Simmons, W. N., Zhu, S. L. and Zhong, P., "Shock Wave Interaction with Laser-Generated Single Bubble," *Physical Review Latter*, **95**, 034501 (2005).
38. Zhu, S. and Zhong, P., "Shock Wave–Inertial Microbubble Interaction: A Theoretical Study Based on the Gilmore Formulation for Bubble Dynamics," *Journal of the Acoustical Society of America*, **106**, pp. 3024–2033 (1999).

(Manuscript received December 22, 2008,
accepted for publication February 10, 2011.)